Flomeko 2000 - IMEKO TC9 Conference
Salvador, Bahia, BRAZIL
4-8 June, 2000

FLOW METER CALIBRATION WITH SONIC NOZZLES IN HIGH-PRESSURE NATURAL GAS

H. Dietrich[1], B. Nath[1], E. v. Lavante[2], M. Jaeschke[3], P. Schley[3], and H.-J. Hotze[3]

[1] Elster Produktion GmbH, Steinernstrasse 19-21, D-55252 Mainz-Kastel, Germany
[2] Institute of Turbomachinery, University of Essen, D-45127 Essen, Germany
[3] Ruhrgas AG, Halterner Strasse 125, D-46284 Dorsten, Germany

Abstract: A new CEN-Standard for gas flow meters requires meters, which working at operating pressures of more than 4 bar to be calibrated accordingly. However in this pressure range, and especially for small flow rates, only a few suitable test rigs exist world-wide. Based on the good experience with sonic nozzles for air at atmospheric conditions, their use for the calibration of gas flow meters in high pressure natural gas is anticipated.

The present paper presents a novel concept for the design and usage of sonic nozzles in high pressure natural gas test rigs. It is based on theory, simulation and measurement results. This concept includes accurate procedures to take into account the gas composition as well as boundary layer and thermal effects of the nozzle flow.

Keywords: Sonic Nozzles, Test Rig, High Pressure, Natural Gas, CFD-Simulation

1 INTRODUCTION

One of the important new regulations of the CEN-standard [1] for gas flow meters is the calibration at the operating pressure when the meter is used at pressures of more than 4 bar. This will cause a significant increase of the number of calibrations done for high pressure natural gas world-wide. Especially gas flow meters with flow rates between Q=1...200m³/h are affected. Unfortunately, high pressure natural gas test rigs usually operate at considerably higher flow rates. Often, the master meters are turbine gas meters or orifices. These types of meters are excellent for large volume flows, but not for the lower ones. A calibration technique which is also excellent for small volume flows is based on critically operated Venturi nozzles. This is one of the most accurate calibration techniques which is very well reproducible and excellently stable in the long term.

To allow a better understanding of this procedure, first of all the details of a critically operated Venturi nozzle as well as the functional principle of the nozzle flow will be described [2].

2 THEORY OF NOZZLE FLOW

The upper part of Figure 1A shows a section of a Venturi nozzle with a toroidal neck. In this case the inlet radius directly turns within the nozzle neck. Since the flow in divergent nozzles tends to cause a separation of the boundary layer and a formation of vortices, an especially small aperture angle of α=4° is chosen (according to ISO 9300 [3]). The exact description of the various flow conditions inside a critically operated nozzle will be provided by means of Figure 1.

In the case that a pressure difference Δp is applied between the inlet and the exit of the nozzle, the flow in the direction of the nozzle neck (index n) can be assumed to have either subsonic or supersonic speed. The actual condition depends on the level of the pressures p_{ni} in the nozzle inlet, p_{ne} in the nozzle exit, and the losses occurring within the nozzle itself. To illustrate these conditions, the centre area B and lower area C of Figure 1 show possible curves of the Mach number M as well as the ratio of static pressure p and total pressure p_t along the nozzle path x for different pressures p_{ne} at the exit of the nozzle – assuming that the nozzle inlet pressure p_{ni} is equal to the total pressure p_t.

If the pressure p_{ne} at the nozzle exit is reduced, by suction, to the value p_{ne1} ($p_{ne1}<p_t$ curve 1), this pressure difference $\Delta p = p_t - p_{ne1}$ leads to a flow in the nozzle. The local Mach number M continuously rises in the convergent inlet of the nozzle and reaches its maximum in the nozzle neck. As the pressure difference Δp is not large enough in order to accelerate the flow within the nozzle

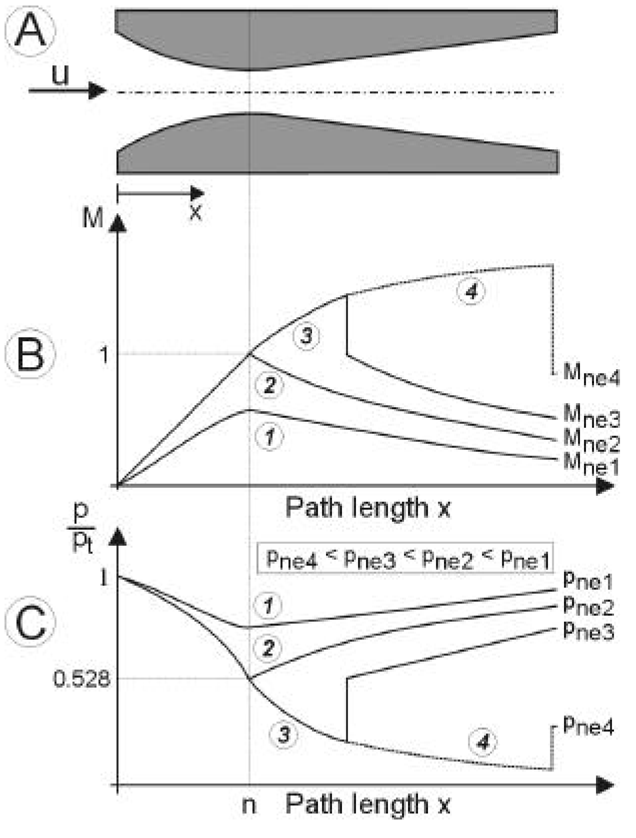

Figure 1. Diagrams of the Mach number M and of the ratio of static pressure p and total pressure p_t along the nozzle path for

neck to the sonic speed c, the divergent part downstream of the nozzle neck n acts as a diffuser and causes a continuous decrease of the local Mach number M. In this case, it is a purely subsonic speed.

The curve ① in the lower area C of Figure 1 shows the associated course of the ratio of static pressure p and total pressure p_t. Due to the conversion of initially potential energy into kinetic energy in the convergent inlet of the nozzle, the pressure ratio p/p_t drops until it reaches its minimum in the nozzle neck. The reduction of the flow velocity u in the diffuser then leads to a reverse conversion of kinetic energy into potential energy. This can be observed by the increase of the static pressure p and hence also of the local pressure ratio of static pressure p and total pressure p_t.

In the case that the pressure at the nozzle exit is reduced to the value p_{ne2} (curve ②) with the inlet pressure being unchanged, the flow within the nozzle neck just reaches sonic speed (M_n=1), and the local pressure ratio within the nozzle neck reaches its critical value of p/p_t=0.528 (cf. Figure 1; curve ②). This condition is termed as the critical flow through the nozzle. The convergent part of the nozzle acts – just as in the case of the pure subsonic speed (curve ①) – as a diffuser and leads to a recovery of the pressure on account of the decreasing Mach number M. Then the mass flow rate q_m through the nozzle reaches its maximum value.

A further reduction of the exit pressure $p_{ne}=p_{ne3}$ (curve ③) first of all accelerates the flow downstream of the nozzle neck to supersonic speed. The discontinuous change of supersonic to subsonic flow is then caused through by a shock wave occurring in the diffuser. By means of an additional reduction of the exit pressure $p_{ne}=p_{ne4}$ (curve ④), the shock wave can be moved to the exit of the nozzle. In such a case, there is a pure supersonic flow.

In the case, the medium remains unchanged it is only dependent on the diameter A_n in the nozzle neck.

The curves in Figure 1 show that the pressure ratio p_n/p_t within the nozzle neck n remains constant and is independent of the outlet pressure p_{ne} when sonic speed (M_n=1) is reached. This relationship is also confirmed by measurements at a nozzle with a diameter of d_n=10 mm within the nozzle neck (cf. Figure 2).

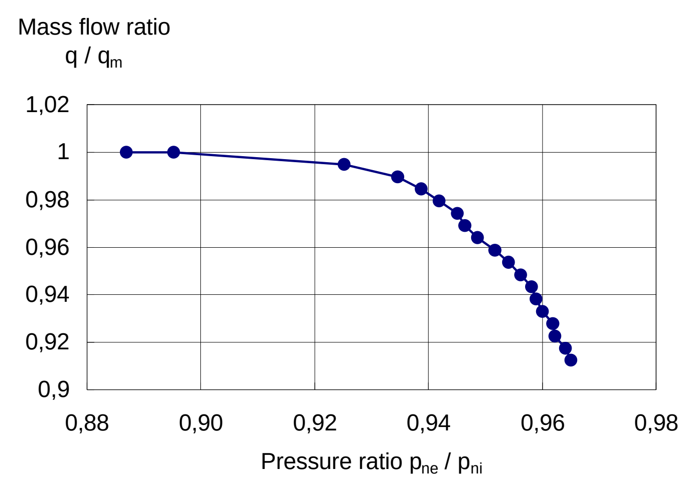

Figure 2. Referenced mass flow q / q_m through the nozzle in dependence of the pressure ratio p_{ne} / p_{ni} along the nozzle.

During this test, air flows under atmospheric conditions through the nozzle. Figure 2 shows the referenced mass flow q / q_m through the nozzle in dependence of the pressure ratio p_{ne} / p_{ni} [1] over the nozzle. In this case, the mass flow through the nozzle at reliable critical condition is used as reference mass flow q_m. The measuring results indicate, that concerning this nozzle, the mass flow remains constant below a pressure ratio of $p_{ne} / p_{ni} = 0.895$ in the nozzle outlet. The flow reaches sonic speed in the nozzle neck n (critical flow). In case of an atmospheric inlet pressure of $p_{ni} = p_t = 1013$ mbar, this corresponds to a pressure difference of $\Delta p = p_{ni} - p_{ne} = 106$ mbar over the nozzle. It is caused by the above-mentioned pressure recovery through the diffuser (cf. curves ①-③ in Figure 1).

The use of sonic nozzles in master meters as a flow reference for gas meter calibration in low and high-pressure applications will be discussed next. For a better understanding, first the low-pressure master meter concept will be described [4].

3 LOW-PRESSURE NOZZLE MASTER FOR AIR

In test rigs operating with air at atmospheric conditions, sonic nozzles are well known for very accurate and reproducible gas meter calibration (Fig. 3).

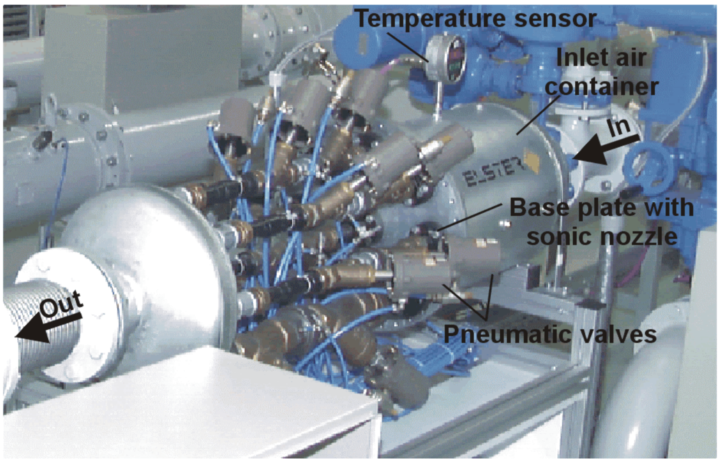

Figure 3. Sonic nozzle prover for flow rates Q=1...250 m³/h integrated in a low pressure test rig for air.

Figure 3 shows, as an example, a nozzle master meter with a set of eight nozzle paths which have a common inlet air container. Since each nozzle can generate only a certain flow, the calibration requires a set of nozzles with each nozzle having a different flow. By using such a set of nozzles, several sections can be connected in parallel – thus providing a large number of different test flow values. This type has a flow range of Q = 1 ... 255 m³/h. The air flows through the test meter into the inlet air container. The individual nozzle sections are connected to the base plate of it. The benefit of this construction consists in the fact that all nozzles take in air from a common chamber whose volume is quasi infinite. The determination of pressure and temperature values upstream of the nozzles therefore requires only one pressure and temperature measuring point in the inlet air container.

Downstream of the nozzle, each pipe is equipped with two shut-off valves to prevent any leakage of the system. By pressurising the gas volume between the two closed shut-off valves, a confident test, that no leakage occurs can be performed.

Provided it is ensured that at least the critical pressure ratio is always applied, the flow will be highly constant. It can be reproduced with a high degree of accuracy and is characterised by a particularly high stability in the long term [5]. Since the nozzle, which is operated in the critical range, directly ensures a constant flow, the load may be adjusted rapidly by opening or closing a nozzle section.

In order to use the high measuring accuracy and reproducibility also in the small flow range, the "small" nozzle master meter has been developed especially for test flows of Q = 0.01 ... 5 m³/h (cf. Figure 4). In general the concept of the small nozzle master meter does not differ from that of the large one.

[1] "ne" corresponds to nozzle exit and "ni" corresponds to nozzle inlet

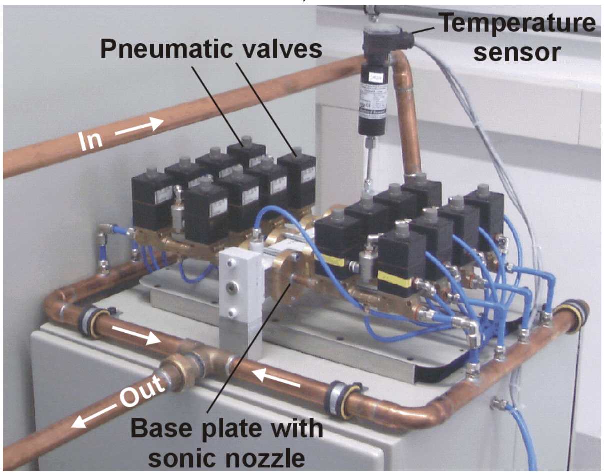

Figure 4. Small sonic nozzle master meter with eight nozzle paths.

Based on positive long time experience with sonic nozzles in test rigs with air at atmospheric conditions [6], the next step will be the use in high pressure natural gas.

4 CALIBRATION IN HIGH-PRESSURE NATURAL GAS

4.1 Theory

In contrast to sonic nozzle applications in air at atmospheric conditions there are some additional characteristics at high pressure natural gas which have to be considered. Equation 1 represents the basic equation to calculate the mass flow Q_m through a critical operated nozzle with the cross sectional area A* in the nozzle throat[2] as well as the density ρ* and flow velocity a* of the medium in the throat.

$$Q_m = A^* \cdot \rho^* \cdot a^* \qquad (1)$$

The real gas behaviour will be expressed with the critical flow function C_*. Usually, values for C_* are given in tables [3] or coefficient equations [7]. Another way to calculate the critical flow function C_* is based on the well known AGA8-DC92 equation [8]. The AGA8-DC92 state equation, has been developed originally to calculate the compressibility factor and density of natural gas in a wide temperature and pressure range. To calculate the calorific values of natural gas based on AGA8, another equation is needed, which describes the calorific behaviour in the state of a perfect gas [9].

Assuming

- isentropic ($s^*=s_0$)
- adiabatic ($h^*=h_0$) flow
- where the flow velocity a* in the throat becomes sonic speed (M=1)

an iterative algorithm can be used and the density ρ* and flow velocity a* of the medium in the nozzle throat can be determined. Then, the critical flow function C_* can be calculated with the stagnation pressure p_0 and temperature T_0 as well as the specific gas constant R_S (equation 2) [10].

$$C_* = \rho^* \cdot a^* \cdot \frac{\sqrt{R_S \cdot T_0}}{p_0} \qquad (2)$$

To take into account the boundary layer effects, the discharge coefficient C_d will be added to equation 1. Equation 3 shows the calculation for the mass flow through critical nozzles under real gas conditions.

---

[2] * is used to mark critical state

$$Q_m = A^* \cdot C_d \cdot C^* \cdot \frac{p_0}{\sqrt{R_s \cdot T_0}} \tag{3}$$

The first experimental use of the algorithm described above for the computation of the critical flow function C_* will be in the high-pressure gas meter test facility *pigsar*.

4.2 Test Set-up

Pigsar is not only an officially approved high-pressure test facility designed for testing and calibrating gas meters used in fiscal metering, but is also since 1999 the official national German standard to define the volume (cubic meter) under high-pressure natural gas conditions. At *pigsar,* flow rates between 8 m³/h and 6,500 m³/h and pressures between 14 bar and 50 bar are provided.

Figure 5 shows a schematic diagram of the *pigsar* test facility.

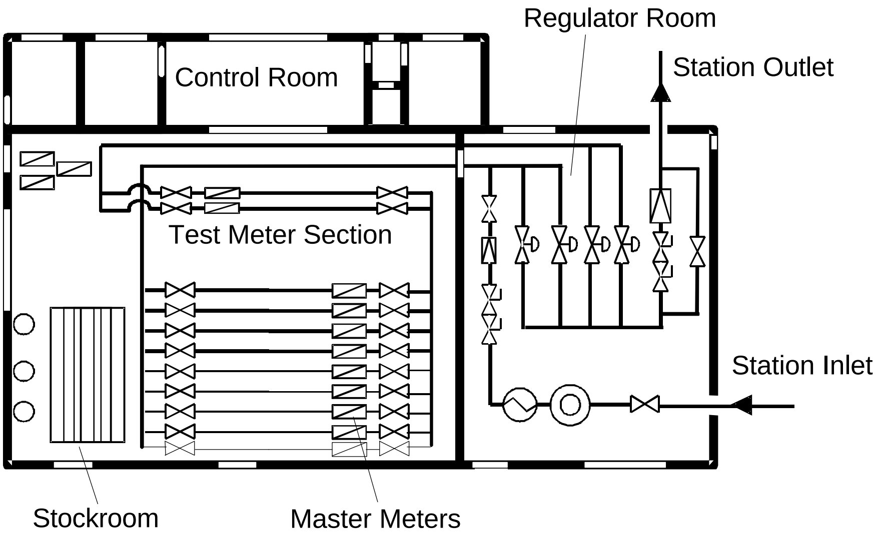

Figure 5. Schematic diagram of the high pressure natural gas meter test facility *pigsar*.

The room on the right comprises the controller and pre-heater facility to adjust gas flow, pressure and temperature. The test rig itself is installed in the room on the left. It consists of 9 turbine gas master meters. (1 master meter G100, 4 master meters G250 and 4 master meters G1000). After leaving the controller and pre-heater facility the gas passes the master meter section before it flows through the test meter. The number of working standards used in parallel, depends on the desired flow rate.

The schematic diagram of the test set-up used for the measurements is shown in figure 6.

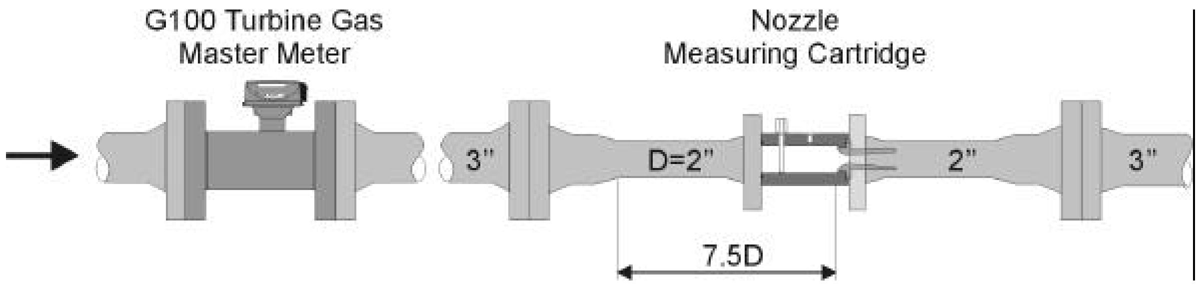

Figure 6. Schematic diagram of the test set-up with working standard and nozzle.

Figure 6 shows the configuration with the flow direction from the left to the right. The nozzle with the inlet and outlet pipe is directly installed in the test meter pipe section downstream of the used

G100 reference turbine gas meter. The inlet pipe length to the master meter is approximately 100 times pipe diameter.

The nozzle section consists of the nozzle itself, an inlet and an outlet pipe section and separate temperature and pressure measuring taps. The pipe diameter is reduced in two steps from 4'' to 2'' in the nozzle inlet. The inlet length of the 2'' pipe to the nozzle inlet is approximately 7.5 times pipe diameter.

The "measuring cartridge" consists of the inlet body with the mounted nozzle clamped between two standard ANSI 600 flanges (figure 7).

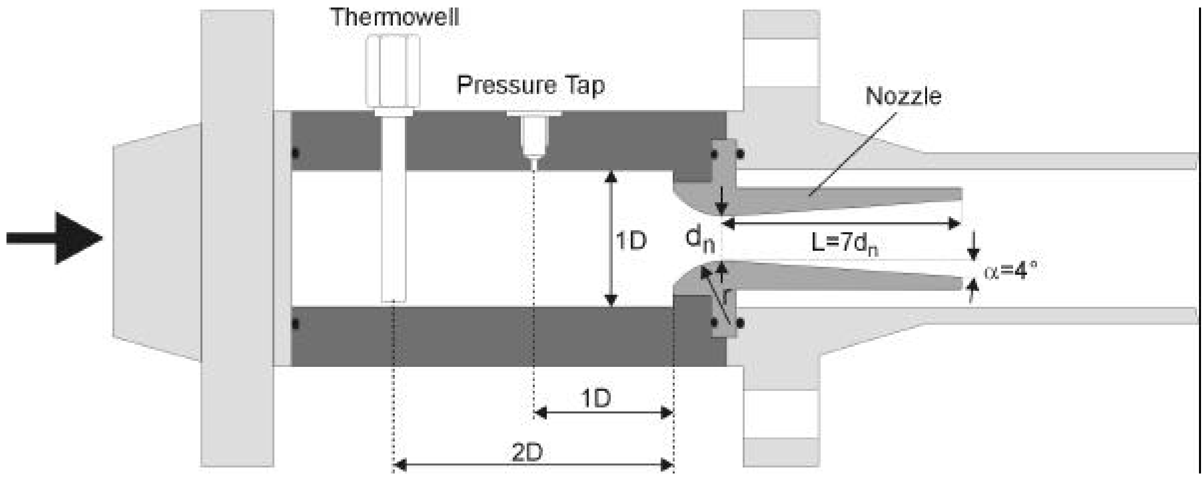

Figure 7. Mechanical drawing of the "measuring cartridge" with temperature and pressure measuring taps and the nozzle itself.

The design of the measuring cartridge is based on national [11] and international standards [3]. To have a smooth axially symmetric run into the nozzle, the nozzle's inlet is precisely machined of stainless steel***.*** The assembly of the nozzle and the inlet is based on a slip on connection. The nozzle inlet has a length of three times pipe diameter and contains the pressure tap as well as a thermowell for the temperature sensor. According to the German PTB[3] test instructions [11] but also concurring with the international DIN EN ISO 9300 standard [3] the distance between the thermowell and the nozzle has been chosen to two times pipe diameter. Between the pressure tap and the nozzle is a distance of one time pipe diameter.

The investigated nozzles have convergent-divergent geometry, with toroidal throats. The divergent part has a length L of seven times throat diameter d, with a divergent wall angle α=4 deg. The inlet radius r of the nozzles is twice of the throat diameter. The exact construction details of the investigated nozzles have been published in 1999 [2].

4.3 Results

Figure 8 shows the nozzle discharge coefficient C_d versus the Reynolds number Re in the nozzle neck. For comparison, several theoretical discharge coefficient C_d curves [3, 12] are shown together with the measuring results of three nozzles under different conditions.

The bold solid curve represents the theoretical discharge coefficient C_d given from the DIN EN ISO 9300 [3] standard and also ASME/ANSI MFC-7M-1987-92 [12] (equation 4).

$$C_d = 0.9935 - 1.525 \cdot \mathrm{Re}^{-0.5} \tag{4}$$

In addition to the main curve, the 0.5 percent tolerance limits are a added.

The dotted lines are based on the American ANSI standard ASME/ANSI MFC-7M-1987-92 Appendix A [12]. The calculation equations published there, distinguish between laminar flow in the nozzle throat (5)

---

[3] PTB = apprevation of "Physikalisch-Technische Bundesanstalt", the German metrological Institute

$$C_d = 0.99844 - 3.032 \cdot \mathrm{Re}^{-0.5} \tag{5}$$

and turbulent flow (6) in the nozzle throat.

$$C_d = 0.99844 - 0.06927 \cdot \mathrm{Re}^{-0.2} \tag{6}$$

Whereas the graph for the turbulent flow lies nearly parallel with a positive offset between the ISO curve and its positive tolerance limit, the curve for the laminar flow (broken line) in the nozzle neck is different to it. In the Reynolds number range $10^5 < \mathrm{Re} < 10^7$ the laminar flow starts nearly at the same value as the main curve (bold solid line). At Reynolds number $\mathrm{Re} \approx 3{\cdot}10^5$ the graph for laminar flow in the nozzle neck crosses the turbulent flow curve and approaches the 0.5 percent tolerance limit. For the Reynolds number range $10^4 < \mathrm{Re} < 10^5$ equation 5 (calculation of the discharge coefficient C_d for laminar flow) is extrapolated (dotted line).

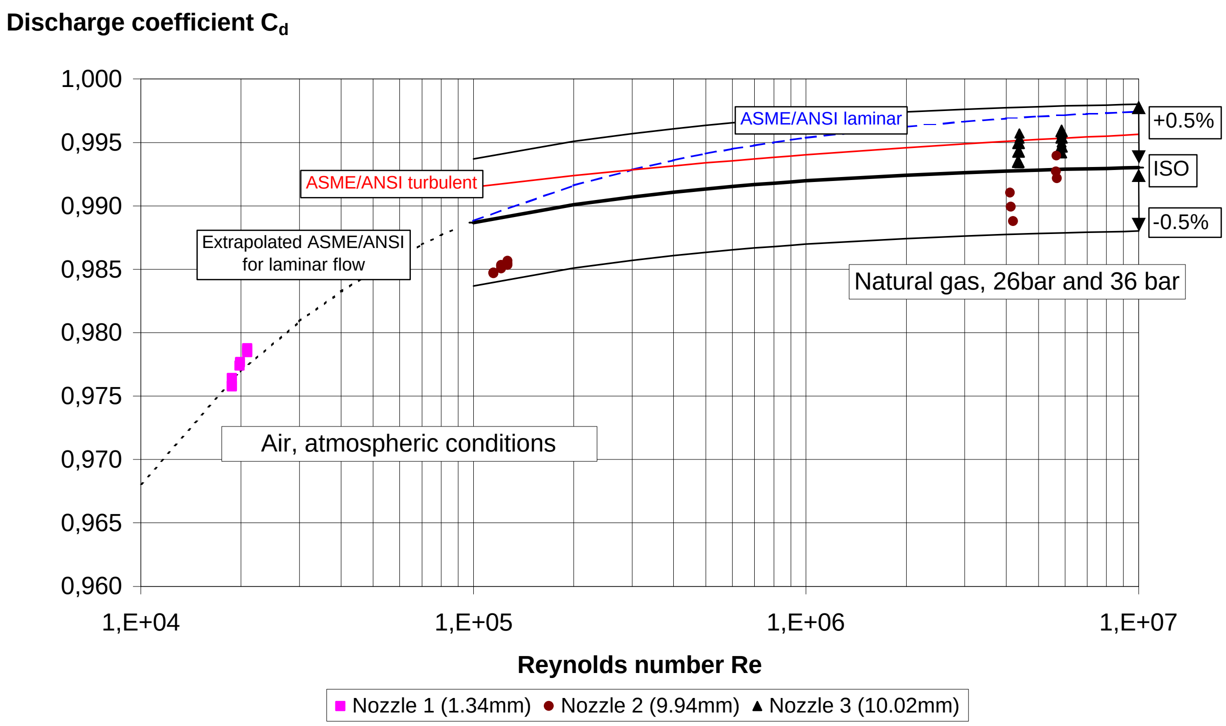

Figure 8. Different theoretical discharge coefficient C_d curves together with measuring results of three nozzles under different conditions.

The measurements in figure 8 are indicated as big sized dots with different shapes. The values for the measured discharge coefficient C_d have been calculated by means of equation 3. For the all flows the measured values from the reference meter are used. The critical flow function C_* in general is calculated with the iterative procedure described above. The static pressure and temperature measurements are taken from nozzle inlet (cf. figure 7) and then converted into the stagnation state. The measurements can be divided into two cases: case I with air at atmospheric conditions and case II with natural gas under high pressure conditions.

The measurements with air are made for nozzle 1 ($d_n = 1.34$mm in throat) and nozzle 2 ($d_n = 9.94$mm) at the PTB. A bell prover is used as master meter. As it can be seen in figure 8, the results for the measured discharge coefficient C_d for the small nozzle 1 in the range of $\mathrm{Re} \approx 2{\cdot}10^4$ matches very well with the extrapolated curve for assumed laminar flow in the nozzle throat (dotted line). The results for nozzle 2 do not fit exactly with the given curves, but are inside the 0.5 percent tolerance limit.

The high-pressure natural gas measurements are in the high Reynolds number range $\mathrm{Re} \approx 4{\cdot}10^6 \ldots 6{\cdot}10^6$. The results at $\mathrm{Re} \approx 4{\cdot}10^6$ were taken at stagnation pressures $p_0 \approx 26$bar and the results at $Re \approx 6 \cdot 10^6$ have been measured at stagnation pressures $p_0 \approx 36$bar. All tests at high-pressure natural gas were made with the test set-up described in chapter 4.2. Nozzle 2 (d_n = 9.94mm) and nozzle 3 (d_n = 10.02mm) were investigated.

All measurement results are close together. Their positions in figure 8 indicate, with regard to the theoretical base curve (bold solid line), that in the high Reynolds number range the theoretical ASME/ANSI nozzle discharge calculation (equation 5 and equation 6 [12]) matches better.

The feasible calibration accuracy using sonic nozzles is not only depending on the exact description of the thermodynamic real gas effects, but also directly from the nozzle discharge coefficient C_d. The development of the boundary layer, causing a change in flow rate and therefore also in the nozzle discharge coefficient C_d has been investigated in a numerical Reynolds number study.

5 BOUNDARY LAYER EFFECTS

The analysed Reynolds numbers are $Re = 1.0 \cdot 10^5$, $Re = 5.0 \cdot 10^5$, $Re = 1.5 \cdot 10^6$ and $Re = 1.0 \cdot 10^7$. The unsteady compressible flow in the nozzle was simulated by the Navier-Stokes solver ACHIEVE, using an upwind biased implicit flux difference splitting scheme [13]. The investigated nozzle has a typical convergent-divergent geometry as mentioned above, with a toroidal throat, and a divergent part of throat diameter length, with a divergent wall angle of α=4 deg. A computational grid such that it was compressed exponentially towards the solid wall was chosen. The resolution was high enough to permit 20 cells within the boundary layer. The pressure ratio across the nozzle for all Reynolds numbers was set to $p_{ne} / p_{ni} = 0.7$

Obviously, in nozzles used for gas metering, the mass flow through the throat is of particular interest. As shown in chapter 2, theoretically, in a choked nozzle, the mass flow in the throat should be constant with time. However, due to the pressure waves traveling upstream, the throat in the smallest nozzle ($Re = 1.0 \cdot 10^5$) is periodically unchocking, resulting in a intermittent decrease of the mass flow. The computed timewise history of the mass flow q_m, non-dimensionalized by the theoretical (inviscid, quasi-onedimensional, ideal nozzle) mass flow q_{mi}, is shown in figure 9 on the left. It should be noted that this expression corresponds to an instantaneous value of the nozzle discharge coefficient C_d.

Interestingly, the higher Reynolds numbers with a corresponding decrease in the boundary layer thickness result in more stable flow conditions. At the Reynolds number $Re = 5.0 \cdot 10^5$, the frequency and amplitude of the unsteady pressure waves are smaller, as indicated by the smaller mass flow than at $Re = 5.0 \cdot 10^5$ fluctuations in figure 9 on the left. At Reynolds numbers $Re \geq 1.5 \cdot 10^6$, the flow in the throat remains choked at all times, as shown by the constant mass flow in the two lower left pictures in figure 9.

The effect of critical Reynolds number on the flow can also be seen in figure 9 on the right. Here the density contours are superimposed by the instantaneous streamlines. At the lowest Reynolds number, the flow is highly unstable in the entire domain, with large vortices due to massive flow separations. With an increasing Reynolds number, the flow becomes more steady and the streamlines smoother. In the case of the highest Reynolds number no vortices are apparent.

The timewise history of static pressure along the nozzle wall for the highest Reynolds number $Re = 1.0 \cdot 10^7$ as a function of time and distance along the nozzle axis is displayed in the lower left of figure 9. Here, the distance L / d_n is referenced to the nozzle diameter d_n starting in the nozzle neck (L / d_n =0) and the time t in $sec \cdot 10^{-2}$. The "smooth" area ahead and slightly behind the nozzle throat should be noticed. Behind the throat, approximately at $L / d_n = 1.6$, a compression shock develops, causing an unsteady pressure and boundary layer.

In the unsteady case, the pressure waves will propagate upstream and cause periodic fluctuation of the mass flow in the throat and at the exit of the nozzle. For short periods of time the flow becomes subcritical with the corresponding decrease of mass flow. This effect causes a decrease in the mean flow rate and consequently also a decrease in the nozzle discharge coefficient C_d. But, because of the high-frequency behaviour with very short unchocked intervals with in parts of milliseconds, for the macroscopic view, which only can be seen from a usual gas meter, the flow conditions are very stable. Therefore, these fluctuations will not affect the use of sonic nozzles as flow reference.

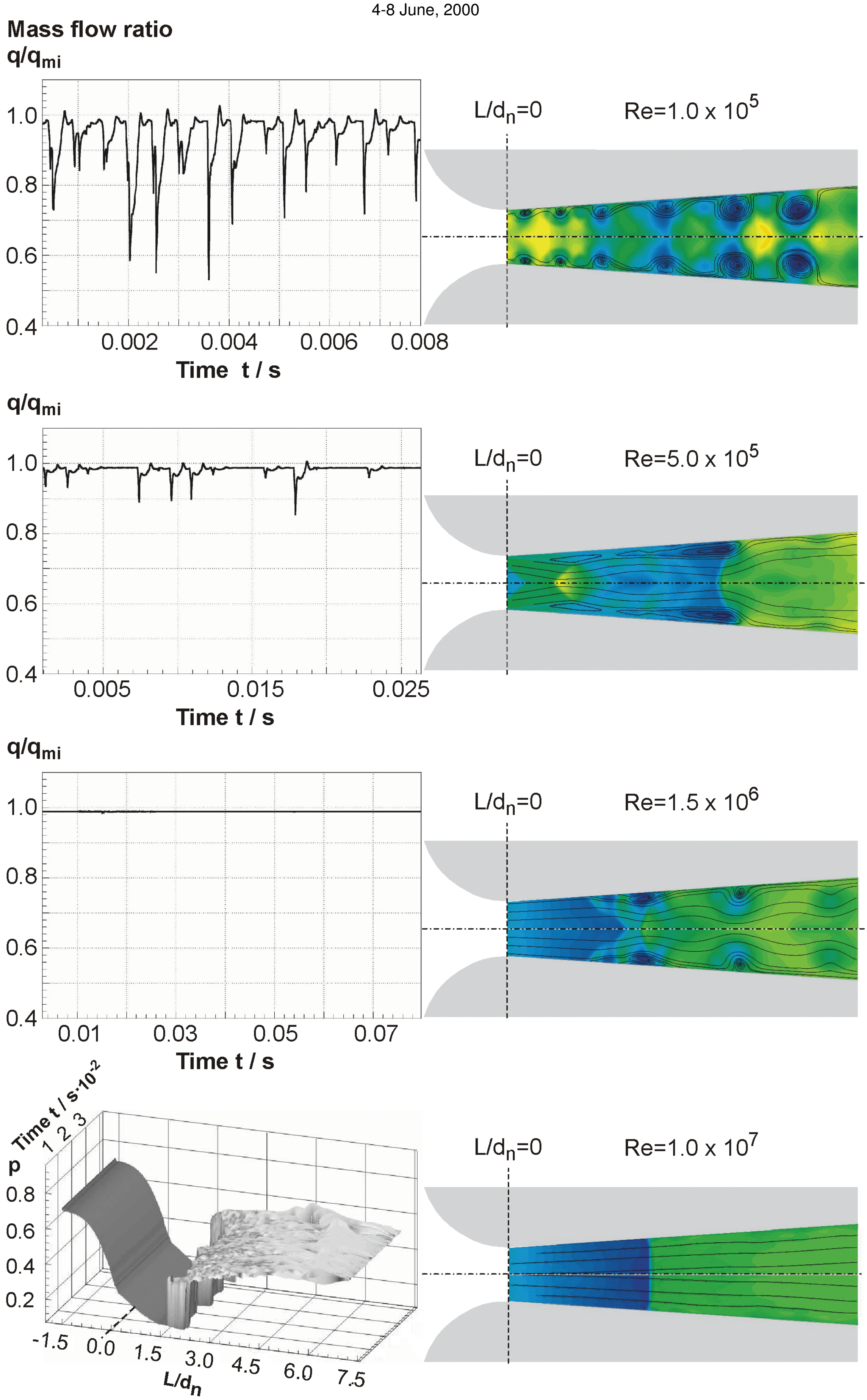

Figure 9. Normalized mass flow as a function of time and density contours with streamlines for four different Reynolds numbers.

6 CONCLUSION

The test rig technology of critically operated nozzles allows the test rig to generate flows and carry out volumetric measurements which are characterized by a maximum long-term stability, reproducibility and accuracy. This is not only the case with air under atmospheric conditions, but also with natural gas under high-pressure conditions.

First measurements with a new kind of calculation for the critical flow function C_* indicate, that the measured nozzle discharge coefficient C_d are in a good agreement with the equations published in the American ANSI standard ASME/ANSI MFC-7M-1987-92 Appendix A [12].

The numerical analysis shows, that depending on the critical Reynolds number the flow in critical nozzles can be highly complex, with possible separated regions and unsteady pressure waves. At Reynolds numbers higher than $Re = 5.0 \cdot 10^5$, the flow in the throat is very stable at critical conditions.

REFERENCES

[1] CEN/TC 237/WG 3, prEN 12261 “Turbine gas meters”, 1998.

[2] H. Dietrich, B. Nath, Test Rigs with Sonic Nozzles for the High-Accuracy Calibration of Gas Flow Meters, in W. Studzinski (ed.), *Proceedings of the International Conference “Fluid Flow Measurement”* (Denver, 27.-30. June 1999), USA, 1999.

[3] International Standard ISO 9300, “Measurements of gas flow by means of critical flow Venturi nozzles”, First Edition, ISO, 1990.

[4] B. Nath, H. Dietrich, Parallel Use of Sonic Nozzles and Turbine Gas Master Meters for High-Accuracy Test Rigs, *Proceedings of the International Conference “FLOMEKO 98”* (Lund, 15.-17. June 1998), Lulea University, Sweden, 1998.

[5] G. Wendt, A. Hartlep, Untersuchungen zur Reproduzierbarkeit des Großgaszählerprüfstandes der Physikalisch-Technischen Bundesanstalt*, PTB-Mitteilungen* 102 (1992) *2*, S. 381-385.

[6] H. Dietrich, B. Nath and E. von Lavante, High-Accuracy Test Rig for Gas Flows from 0.01 m³/h up to 25 000 m³/h, *Proceedings of the International Conference “IMEKO 99”* (Osaka, 13.-18. June 1999), Osaka, Japan, 1999.

[7] R. C. Johnson: Calculation of the Flow of Natural Gas Through Critical Flow Nozzles. *Journal of Basic Engineering* 92 (1970) No. 3, 580-589.

[8] K. E. Starling, and J. L. Savidge: Compressibility Factors of Natural Gas and Other Related Hydrocarbon Gases. “*American Gas Association Transmission Measurements Committee Report No. 8*”, Second Edition, Arlington 1992 and Errata No. 1, June 1993.

[9] M. Jaeschke, P. Schley, Ideal-Gas Thermodynamic Properties for Natural Gas Applications,*“International Journal of Thermophys.”,* Vol. 16(1995)6*,* Germany, p. 1381-1392.

[10] P. Schley, E. von Lavante, D. Seitz, M. Jaeschke, H.Dietrich and B. Nath: Simulation of Critical Nozzle Flow Considering Real Gas Effects. *Proceedings of the International Conference “FLOMEKO 2000”* (Salvador, 4.-8. June 2000), Salvador, Bahia, Brasil, 2000.

[11] G. Wendt, H. Dietrich, F. Frössl, B. Jarosch, R. Joest, B. Nath, M. Ruwe, PTB-Prüfregeln: *"Prüfstände mit kritisch betriebenen Düsen für Luft"*, Physikalisch-Technische-Bundesanstalt, Braunschweig, 1998.

[12] American National Standard ASME/ANSI MFC-7M-1987, “Measurements of Gas Flow by Means of Critical Flow Venturi Nozzles”, American Society of Mechanical Engineers, 1987.

[13] E. von Lavante, A. El-Miligui, F. Cannizzaro and A. H. Warda, Simple Explicit upwind Schemes for Solving Compressible Flows, *Proceedings of the 8th GAMM Conference on Numerical Methods in Fluid Mechanics”*, Delft, Netherlands, 1990

AUTHORS:

[1] Elster Produktion GmbH, Research and Development, Steinernstrasse 19-21, D-55252 Mainz-Kastel, Germany, Phone Int ++49 6134 605 356, Fax: ++49 6134 605 490, E-mail: dietrich@elster.com, nath@elster.com

[2] Institute of Turbomachinery, University of Essen, D-45127 Essen, Germany, Phone Int ++49 201 183 2285, Fax: ++49 201 183 2285, E-mail: erni@tigger.turbo.uni-essen.de

[3] Ruhrgas AG, TAM, Halterner Strasse 125, D-46284 Dorsten, Germany, Phone Int ++49 2362 93 8570, Fax: ++49 2362 93 8606, E-mail: Manfred.Jaeschke@ruhrgas.com, Peter.Schley@ruhrgas.com; Hans-Juergen.Hotze@ruhrgas.com